Both adaptive immunity and IL-1R1 dependent signals improve clearance of cytosolic virulent mycobacteria *in vivo.*

Authors / Affiliations

Sanne van der Niet[1], Maaike van Zon[2], Karin de Punder[2,3], Anita Grootemaat[1], Sofie Rutten[1], Simone Moorlag[2], Diane Houben[2], Astrid van der Sar[4], Wilbert Bitter[4], Roland Brosch[5], Rogelio Hernandez Pando[6], Maria T. Pena[7], Eric A. Reits[1], Katrin D. Mayer-Barber [8] and Nicole N. van der Wel[1*]

Contact information

[1] Electron Microscopy Centre Amsterdam, Amsterdam University Medical Centre AMC, the Netherlands, [2] Netherlands Cancer Institute, The Netherlands, [3] Charité - Universitätsmedizin Berlin, Germany, [4] Amsterdam University Medical Centre VUMC, The Netherlands, [5] Unit for Integrated Mycobacterial Pathogenomics, CNRS UMR 3525, Paris, France, [6] National Institute of Medical Sciences and Nutrition, Mexico, [7] Department of Health and Human Services, Health Resources and Services Administration, Healthcare Systems Bureau, National Hansen's Disease Programs, Baton Rouge, LA, USA [8] Inflammation and Innate Immunity Unit, Laboratory of Clinical Immunology and Microbiology, National Institute of Allergy and Infectious Diseases (NIAID), National Institutes of Health (NIH), Bethesda, USA;

*Corresponding author: Nicole van der Wel

email address: n.n.vanderwel@amsterdamumc.nl

Summary

Mycobacterium tuberculosis infections claim more than a million lives each year and better treatments or vaccines are required. A crucial pathogenicity factor is translocation from the phago-lysosomes to the cytosol upon phagocytosis by macrophages. The translocation from the phago-lysosome into the cytosol is an ESX-1 dependent process as previously shown *in vitro*. Here we show that *in vivo,* mycobacteria also translocate to the cytosol but mainly when host immunity is compromised. We observed only low numbers of cytosolic bacilli in mice, armadillo, zebrafish and patient material infected with *M. tuberculosis, M. marinum* or *M. leprae*. In contrast, when innate or adaptive immunity was compromised, as in SCID or IL-1R1 deficient mice, a significant number of cytosolic *M. tuberculosis* bacilli were detected in lungs of infected mice. Taken together, the cytosolic localization of mycobacteria *in vivo* is controlled by adaptive immune responses as well as IL-1R1-mediated host resistance to *M. tuberculosis*.

Keywords: *Mycobacterium tuberculosis*, *Mycobacterium leprae*, *Mycobacterium marinum*, cytosolic localization, IL-1 receptor 1, phagosome, lysosome, phago-lysosomal fusion.

Introduction

Mycobacterium tuberculosis (*Mtb*) is not only one of the most deadliest pathogens in history, but it continues to claim an estimated 1.5 million human lives per year (World Health Organization, 2019) and is a big threat for the future as multidrug resistant strains are arising with no effective treatment nor vaccine available. The treatment success rate is just 56% and in approximately 6.2% of the cases, infection is caused by extensive drug resistant *Mtb* (World Health Organization, 2019). Furthermore, *Mtb* is the leading cause of death among HIV infected patients. In patients with AIDS, tuberculosis can thrive because their immune system is impaired by $CD4^+$T cell loss, which secondarily affects many other immune compartments (reviewed in Doitsh & Greene, 2016).

For an effective response to *Mtb* infections, both the innate and the adaptive immune system are important. The development of an active pulmonary *Mtb* infection is related to a disordered

immune balance, which results in the inability of the host to keep the infection under control (Queval, Brosch, & Simeone, 2017). The first immune response is the innate response (reviewed in Lerner, Borel, & Gutierrez, 2015) including a series of cells that come in contact with *Mtb* such as alveolar macrophages. Alveolar macrophages provide a nutritionally permissive niche (Huang, Nazarova, Tan, Liu, & Russell, 2018) and are critical for dissemination of the bacteria in the lung, spreading the infection from the alveoli to the interstitium (Cohen et al., 2018). Here *Mtb* infects other cell types like neutrophils, monocyte derived macrophages and dendritic cells (DC). Since DCs present antigens via MHC class I and II to T cells, they function as a connection between the innate and adaptive immune system (Marino et al., 2004; Sayes et al., 2018). Upon antigen presentation to T cells, $CD4^{+}$T cells produce IFNγ, which is involved in the enhancement of macrophage killing and plays an important role in granuloma formation (Muruganandah, Sathkumara, Navarro, & Kupz, 2018). Indeed in mice (Flynn et al., 1993) and humans (Dupuis et al., 2000) loss of IFNγ or its receptors, acting as single non-redundant factor, leads to TB disease. In order to spread to new individuals, *Mtb* needs to cause pulmonary lesions (Guirado et al., 2015). Inflammation driven by IL-1 contributes to host resistance to *Mtb* (Bohrer, Tocheny, Assmann, Ganusov, & Mayer–Barber, 2018; Mayer-Barber et al., 2014). Mice that lack the IL-1R1, IL-1α or IL-1β display high susceptibility to *Mtb* infection (Mayer-Barber et al., 2011) with uncontrolled bacterial replication in the lungs, again demonstrating a non-redundant role of one key host pathway.

We hypothesized that bacterial translocation from the phagosome to the cytosol might also be regulated by IL-1. *In vitro, Mtb* can translocate from the phago-lysosome to the cytosol (Houben et al., 2012; Leake, Myrvik, Wright, & Carolina, 1984; Lerner et al., 2016, 2018, 2020; Mcdonough, Kress, & Bloom, 1993; Simeone et al., 2012; van der Wel et al., 2007) in an ESX-1 dependent manner (Houben et al., 2012; Simeone et al., 2012; van der Wel et al., 2007). This system is responsible for the secretion of a number of proteins, including EsxA (ESAT-6) and EsxB (CFP-10) (reviewed in Vaziri and Brosch, 2019). When this secretion system is not

present, as is the case for *M. bovis* BCG, cytosolic localization is abrogated in *in vitro* macrophage systems, rendering the bacteria restricted in a membrane enclosed phago-lysosome. Reintroducing the extended *esx-1* locus in BCG allowed the translocation to the cytosol and increased virulence providing clear evidence for an essential role of this Type VII secretion system in escape (Augenstreich et al., 2017; Gröschel et al., 2017; Houben et al., 2012; Kupz et al., 2016; Pym et al., 2003). In addition, it is shown that virulent *Mtb* can form cords in the cytosol and not in the phagosome in human lymphatic endothelial cells *in vitro* (Lerner et al., 2020). This cording is dependent on the ESX-1 secretion system and PDIM glycolipids. The formation of cords in the cytosol rather than in phagosomes suggests a permissive environment for bacterial replication in the cytosol. When *Mtb* is present in the cytosol its bacterial DNA is sensed by cyclic guanosine monophosphate-AMP synthase (cGAS) (Collins et al., 2015; Majlessi & Brosch, 2015; Wassermann et al., 2015; Watson et al., 2015). This detection is dependent on the presence of a functioning ESX-1 system, suggesting that it is dependent on pathogen-induced cytosolic localization. Cytosolic bacteria co-localize with cytosolic ubiquitin, while this is not the case when the mycobacteria are present in the phagosome (Houben et al., 2012). Another factor involved in the cytosolic localization is Rv3167c, which regulates the escape of *Mtb* from the phagosome, since a mutant unable to produce this protein (MtbΔRv3167c) displayed increased cytosolic escape (Srinivasan et al., 2016). Other virulent factors involved in escape from the phagosome are PDIM glycolipids located on the outer membrane of *Mtb* (Augenstreich et al., 2017; Lerner et al., 2018; Quigley et al., 2017). Mycobacterial strains that lack PDIM are less capable of damaging the phagosomal membrane, resulting in less *Mtb* in the cytosol of THP-1 macrophages.

While most studies focused on *in vitro* experiments using cultured macrophages, the sub-cellular localization of *Mtb* and the factors affecting cytosolic localization and pathogenesis are less intensively studied *in vivo*. When macrophages purified from bronchoalveolar lavages from TB infected patients were analyzed by electron microscopy, it was found that *Mtb* is primarily localized in phagosome-like compartments (Mwandumba et al., 2004; Russell,

Mwandumba, & Rhoades, 2002). The phagosomal localization does not affect the ability of *Mtb* to proliferate, and it is long known that when *Mtb* is located in phagosomes it is able to arrest its maturation (Armstrong & D'Arcy Hart, 1971; Sturgill-Koszycki et al., 1994) up to 5-7 days (Sundaramurthy et al., 2017). More recently, it was shown *in vivo* that *Mtb* is able to translocate to the cytosol as early as three hours post infection using a Förster resonance energy transfer (FRET)-based detection system (Simeone, Sayes, Song, Gröschel, & Brodin, 2015). This study also demonstrated that the pH of the lysosomes plays a role in the cytosolic localization; when the lysosome is more acidic, less *Mtb* is present in the cytosol at 3 days post infection (Simeone et al., 2015).

To examine whether activation via adaptive or innate immunity pathways would affect the capability of mycobacteria to translocate into the cytoplasm *in vivo,* we tested the subcellular localization of different mycobacterial species in zebrafish, armadillo and mice models as well as in patient material. In adult zebrafish and zebrafish embryos we used *M. marinum*, a close homologue of *Mtb* that is also known to escape the phago-lysosome in an ESX-1 dependent manner (Stamm et al., 2003). *M. leprae* is also known to escape to the cytosol (van der Wel et al., 2007), probably using a similar mechanism, although some of the members of ESX-1 system (like esxC, esxG, esxS) are pseudogenes, it has functional ESAT-6 (esxA) and CFP-10 (esxB), the two most important components needed for cytosolic escape. We used both skin biopsies of leprosy patients and the armadillo model for *M. leprae* since, the armadillo model is known to exhibit the entire clinical spectrum of leprosy (Sharma et al., 2013). For *Mtb* both SCID mice that lack both T and B cells, and IL-1R1 knockout mice were compared to determine their ability to limit cytosolic escape *in vivo* in infected cells. Here we show that while cytosolic localization is limited by both innate and adaptive immunity, IL-1 seems to be a key effector pathway in controlling cytosolic translocation of *Mtb*.

Results

The pH of the phagosome and lysosome does not affect cytosolic localization of *M. marinum*.

Mtb blocks maturation and acidification of the phago-lysosome, promoting its intracellular survival (Armstrong & D'Arcy Hart, 1971; Clemens, Lee, & Horwitz, 2000; Russell, Vanderven, Glennie, Mwandumba, & Heyderman, 2009; Sturgill-Koszycki et al., 1994; Wong, Bach, Sun, Hmama, & Av-gay, 2011). Phagosomal acidification is essential for increased activity of the lysosomal digestive process and thus for degradation of its content (Vieira, Botelho, & Grinstein, 2002). *Mtb* partially avoids acid mediated killing by blocking fusion between lysosomes and phagosomes (Mwandumba et al., 2004; Sturgill-Koszycki et al., 1994) and the secretion of antacid known as 1- tuberculosinyladenosine (TbAd) (Buter et al., 2019). In addition, it is shown that the mycobacterial cell wall plays a role in the resistance to acidic environments (reviewed in Vandal et al., 2009). We hypothesized that cytosolic escape is a fourth mechanism to avoid lysosome mediated killing. To determine whether these mechanisms are interdependent, we examine if the phagosomal pH affects translocation from the phagosome to the cytosol. To exclude the effect of TbAd, we utilized *M. marinum*, which does not express TbAd (Young et al., 2015) in THP-1 cells. The acidity of the phagosome and the lysosome was measured using lysotracker and by incubation with (N-(3-((2,4-dinitrophenyl)amino)propyl)-N-(3-aminopropyl) methylamine (DAMP), a weak basic amine that will be taken up by acidic organelles in live cells (Mwandumba et al., 2004). After fixation and sample preparation, the DAMP was visualized by Transmission Electron Microscopy (TEM) using immuno-gold labelling with αDNP antibody conjugated to a gold particle. The more acidic the phagosome or lysosome, the more DAMP was present, thus resulting in a higher label density in acidic organelles. As expected, upon *M. marinum* infection of THP-1 cells, low amounts of DAMP labelling were observed surrounding cytosolic *M. marinum* (Supplemental Figure 1A/1A') while more labeling was detected in *M. marinum* containing phagosomes

(Supplemental Figure 1A/1A"). We next blocked acidification with 10nM Concanamycin B (ConB), an inhibitor of vacuolar ATPases which prevents acidification of endosomes and lysosomes. When cells were treated with ConB and infected with *M. marinum,* both a lower label density was measured and the lysotracker imaged with fluorescence microscopy confirm that the pH is less acidic in the phagosome/lysosome when treated with ConB as already well described (Crowle, Dahl, Ross, & May, 1991; Mwandumba et al., 2004) (Supplemental Figure 1B). We next examined whether a raising pH would affect the translocation efficiency of *M. marinum* to the cytosol. The percentage of cytosolic bacteria in THP-1 cells treated with ConB or no treatment control was determined both at 24h and 48h after infection with *M. marinum,* which is the known timeframe for escape (Houben et al., 2012) (Figure 1A,B). The number of bacteria present in CD63 labeled compartments (phago-lysosomal), membrane enclosed but not CD63 positive compartments (phagosomes) and the number of bacteria in the cytosol were counted (Supplemental Figure 2A). At both 24h and 48h after infection no difference in the percentage cytosolic bacteria was detected for untreated or ConB treated cells. This indicates that a higher pH has no effect on *M. marinum* translocation to the cytosol. In conclusion, a raised lysosomal pH has no effect on the percentage of bacteria translocating to the cytosol in THP-1 cells.

M. marinum translocates to the cytosol in embryonic but not adult zebrafish.

After studying the effect of the pH on the ability of *M. marinum to* translocate to the cytoplasm *in vitro*, we next focussed on the subcellular localisation *in vivo*. To address whether either adaptive or innate immunity was required to limit bacterial cytosolic escape we used a zebrafish model combined with *M. marinum* infection. Among other age-related differences, zebrafish larvae do not have a fully developed adaptive immune system in contrast to adult zebrafish (Langenau et al., 2004). Zebrafish embryos and adult zebrafish were infected with *M. marinum* or *M. marinum* Tn::ESX5 mutant and tissue was fixed for TEM analysis. For analysis of adult zebrafish a specific *M. marinum* Tn::ESX5 mutant was used as this infection

was shown to cause hypervirulence (Weerdenburg et al., 2012) and thus large amounts of bacteria can be detected *in vivo* using TEM. The following conditions were analysed using TEM: whole zebrafish embryo day 9 and the spleen of adult zebra fish at day 11 (Figure 2A,B). The percentage of cytosolic *M. marinum* was determined by counting the number of mycobacteria in a membrane enclosed compartment and in the cytoplasm. Discrimination between phagosome and phago-lysome based on immuno-gold labelling with lysosomal markers available in humans or mice (CD63, LAMP1) was not possible as no lysosomal markers are available for immuno-gold labelling in zebrafish. Alternatively, actin antibodies were used as a cellular cytoskeleton marker. In embryos infected for 9 days 32% of *M. marinum* was present in the cytosol (Figure 2C and Supplemental Figure 2B). Out of the four adult zebrafish analyzed, one was discarded as no bacteria could be deteced. In the other three fish ample bacteria were detected and catagorized as phagosomal or cytosolic based on the presence of membrane. In adult zebrafish less than five percent of the bacteria were found in the cytosol (Figure 2C). Thus, adult but not embryo zebrafish were able to limit bacterial cytosolic escape. This outcome suggests the presence of an adaptive immune system promotes bacterial containement in the phago-lysosome, although other age related factors could be at play.

Cytosolic localization of *M. leprae* is restrained in both armadillo and patient skin

To examine whether cytosolic localization can only be detected in early, innate stages of infections, we used another model organism; *M. leprae*, the causative agent for leprosy. Like *Mtb*, these bacteria have been shown to translocate to the cytosol in an *in vitro* model (van der Wel et al., 2007). We studied early (day 3) and late stage (day 21) infections in armadillos and in addition, biopsies were taken from 4 lepromatous leprosy (LL) patients with a well-established infection. The skin of the abdomen of armadillos was infected with both unviable (irradiated) as well as viable *M. leprae.* At the site of infection, loss of pigment was visible which increased during infection progression (Figure 3A and B). No differences were observed in loss of pigment between the sites infected with irradiated *M. leprae* and viable *M. leprae*. At

the border of pigment loss, armadillo skin biopsies infected with viable *M. leprae* were fixed for TEM analysis, to determine if the localization of the bacteria is cytosolic versus phagosomal. Immuno-gold labelling against *M. leprae* specific anti-Cell Wall Protein was used to verify that these are indeed mycobacteria. Similar to the localization of *M. marinum* in adult zebrafish, the majority of the bacteria were present in membrane enclosed phagosomes and cytosolic bacteria were only occasionally detected at both day 3 (Figure 3C) and 21 after infection. In addition, skin biopsies of 4 different lepromatous leprosy patients taken from the border of the infection as defined by the depigmentation line and were analyzed using TEM and immuno-gold labelling for *M. leprae* specific anti-Cell Wall Protein and lysosomal markers such as Cathepsin D (Figure 4), LAMP1, and CD63. From the 4 patients, individual bacteria were detected and classified for their subcellular localization based on the presence of surrounding membrane and 2 or more gold particles detecting Cathepsin D (Supplemental Figure 2C). Similar to the armadillo and adult zebrafish, the percentage of cytosolic mycobacteria was low (1.1%), while over 700 bacilli were assessed. In conclusion, in both armadillo and human skin, a low percentage of cytosolic *M. leprae* bacteria is present at all measured stages of infection.

Immunocompetent BALB/c, but not SCID mice can contain *M. tuberculosis* inside phagosomes of infected pulmonary cells.

After showing that neither *M. leprae* nor *M. marinum* translocate in high numbers to the cytosol even at later stages of infection, we next wanted to study the subcellular localization of *M. tuberculosis* longitudinally in mice. To do so BALB/c mice were infected with the virulent *Mtb* strain H37Rv and lung tissue was fixed for EM analysis at day 2, 7, 21, 45 and 120 after infection. These samples were immunogold labelled for lysosomes using LAMP1 or Cathapsin D and imaged using TEM (Figure 5). As for *M. marinum* in THP1 cells and *M. leprae* in skin, the number of bacteria present in LAMP-1 labeled phago-lysosomes, membrane enclosed but not LAMP-1 labelled phagosomes and the number of bacteria in the cytosol were counted (Supplemental Table 1). We found that cytosolic localization was highest at day 7 of infection,

with still less than five percent of *Mtb* detectable in the cytosol and most bacteria residing in a membrane enclosed compartment. To determine if patient derived strains behave similar to H37Rv, BALB/c mice were infected with two additional *Mtb* strains from lineage 2, often referred to as Beijing family *Mtb* (1998-1500 ancient Beijing) and multi drug resistant strain (2002-0230 Beijing). EM analysis was done at 21, 45 and 120 dpi and demonstrated also low amounts cytosolic bacteria (Supplemental Table 1). Thus, as shown previously in immune-competent mice, different strains of *Mtb* reside primarily inside membrane enclosed compartments and not inside the cytosol.

To directly address a potential contribution of the adaptive immune system we next quantified *Mtb* cytosolic translocation in SCID mice. SCID mice lack functional T and B cells, key mediators of adaptive immunity in vertebrates and succumb rapidly to *Mtb* infections. SCID mice were infected with *Mtb* strain H37Rv via aerosol and killed 21 days after infection. Lungs were then fixed and processed for EM analysis and sections labelled for LAMP1 using immuno-gold labelling to indicate lysosomes and phago-lysosomes (Supplemental Table 1). We detected a 10-fold increase in *Mtb* cytosolic translocation in SCID compared to BALB/c mice, arguing that T and B cells are required for optimal exclusion of bacilli from the cytosol of infected cells.

Mtb is preferentially located in the cytosol of infected pulmonary cells in IL-1R1 deficient mice

IL-1 is a potent innate inflammatory cytokine critically required for resistance against bacterial infections. Mice deficient in the IL-1 pathway, such as IL-1α and IL-1β are highly susceptible to *Mtb* infection with increased mortality and bacterial growth in lung and spleen and development of necrotic granulomatous lesions that more closely resemble human necrotic lesions (Juffermans et al., 2000; Mayer-Barber et al., 2011, 2014, 2010; Yamada, Mizuno, Horai, Iwakura, & Sugawara, 2000). To investigate the contribution of this innate immune pathway in the prevention of mycobacterial cytosolic escape, we infected *Il1r1-/-* and B6 WT

mice with *Mtb* and 4 weeks after infection fixed lung tissue and processed it for TEM analysis. As Mtb is normally difficult to find, first fluorescence microscopy was performed and tissues were sectioned at 200 nm and stained for detection of nuclei and mycobacteria (Figure 6 A,B) to be able to select for the infected area (van Leeuwen et al., 2018). Whereas in B6 mice only small spots of *Mtb* are detected (like for BALB/c mice), infected *Il1r1-/-* tissue is heavily labelled and thus infected. Ultrathin sections were labelled for LAMP1 and CD63 using immuno-gold labelling to indicate lysosomes and phago-lysosomes for TEM analysis. As before, difference between phago-lysosomal, phagosomal and cytosolic *Mtb* was determined based on the presence of immuno-gold labelling and a membrane surrounding the bacteria (Figure 6C,D and Supplemental Figure 2D). *Mtb* was found in the phago-lysosome, the phagosome and in the cytosol. Strikingly, we detected a 14-fold increase in the number of *Mtb* translocated to the cytosol in *Il1r1-/-* deficient lungs compared to WT B6 lungs infected with *Mtb*. While only 2.5% of *Mtb* bacilli were located in the cytosol in the lungs of infected WT B6 mice, over 30% of the *Mtb* bacilli in the lung were able to escape to the cytosol in the absence of IL-1 signaling. Thus, IL-1 dependent signals are required to prevent cytosolic localization of *Mtb.*

Discussion

The cytosolic localization of mycobacteria has been debated ever since the first description in the late 1980s (Leake et al., 1984; Mcdonough et al., 1993; Myrvik, Leake, & Wright, 1984). Our immuno-gold TEM analysis of *Mtb*, BCG and mutant strains in 2007 (van der Wel et al., 2007) restarted the discussion and several studies have now confirmed the presence of extra-phagosomal *Mtb* bacilli (Houben et al., 2012; Simeone et al., 2012, 2015). In addition, the release of DNA into the cytosol was described and is, like escape from the phagosomal compartment, dependent on the ESX-1 secretion system (Collins et al., 2015; Wassermann et al., 2015; Watson et al., 2015). In this study, we showed that *in vivo, Mtb* is mainly present in membrane bound compartments and not in the cytosol of infected cells. This also holds true for the pathogenic mycobacteria, *M. leprae* and *M. marinum.*

Here, we showed that raising the lysosomal pH did not affect cytosolic localization of *M. marinum*. In THP-1 cells, *M. marinum* can escape irrespective of the raised pH of the lysosome. As well-known already, maturation of the *Mtb* phagosome is altered (Armstrong & D'Arcy Hart, 1971; Clemens et al., 2000; Russell et al., 2009) and our data suggest that the pH of phagosomes has no effect on translocation. Simeone and collegues (2015) showed *in vivo* that when phagosomal acidification was blocked using bafilomycin, an induction of mycobacterial access to the cytosol is detected. Therefore, we hypothesized that raising the phagosomal and lysosomal pH by ConB would result in increased cytosolic localization of *M. marinum*. However, we found at a cellular level, no difference in the percentage of cytosolic *M. marinum.* Our cell-culture derived data merely demonstrate that mycobacteria can translocate irrespective of the pH, and thus manipulation of the pH by ConB did not change the subcellular localization in cells under *in vitro* conditions. Importantly, *in vivo,* as studied here and by Simeone et al., (2015), subcellular localization of mycobacteria is a highly complex and dynamic process.

After inhalation in the lung, *Mtb* is initially taken up by alveolar macrophages and spreads among innate immune cells while delaying the initiating adaptive immunity (Mayer-Barber & Barber, 2015; Rothchild et al., 2019; Samstein et al., 2013). Importantly, both innate and adaptive immunity are critically important for optimal host resistance against *Mtb*. Here, we show that while the lysosomal pH itself has a minimal role, effective adaptive and innate host immunity play a critical role in preventing mycobacterial escape to the cytosol. The delicate balance between bacterial replication and containment by the host immune response is lost when immunity is compromised by either lack of T and B cells in SCID mice, or even more dramatically, in the absence of innate IL-1R1 signaling. Of note, the profound increase in IL-1R1 deficient mice exceeds moderate but significant increase in SCID mice, even though the former likely has a broader set of immunological defects. This may argue that despite increased susceptibility to *Mtb*, certain specific immune pathways like IL-1 may be more directly and preferentially involved in regulating cytosolic escape. In line with our observations

in SCID and IL-1R1 deficient mice, we further propose that *Mtb* has a limited ability to escape to the cytoplasm when the immune system is intact. However, this limited ability still results in rare cytosolic escape events, which likely may lead to activation of cytosolic immunosurveillance pathways, including those linked to IL-1, which promote rapid clearance by the immune cells attracted to infected cells.

Cytosolic immunosurveillance pathways are triggered by pathogens directly or by pathogenic products entering the cytosol, and are often linked to anti-viral immunity and type I IFN induction as well as inflammasome activation. Inflammasomes are cytosolic signaling complexes that ultimately lead to cytolytic cells death and IL-1 family cytokine processing. It is now established that bacterial DNA can translocate to the cytosol, in an ESX-1 dependent manner, where it is detected by cytosolic DNA sensors such as cGAS and AIM2 (Collins et al., 2015; Kupz et al., 2016; Wassermann et al., 2015; Watson et al., 2015) cGAS in turn synthesizes a second messenger (cGAMP) which activates the STimulator of IFN Genes (STING) and type I IFN signaling and expression of IFN-α and β (reviewed in Chen et al., 2016). When cytosolic DNA is detected by AIM-2, the NRLP3 inflammasome is activated and leads to proteolytic cleavage of IL-1β (Collins et al., 2015; Kupz et al., 2016; Wassermann et al., 2015; Watson et al., 2015). We have previously shown that IL-1 and type I IFNs exhibit potent cross regulation important for host resistance against Mtb with excessive type I IFN induction in the absence of IL-1 signaling (Ji et al., 2019; Mayer-Barber et al., 2011, 2014). The elevated type I IFNs expression in the absence of IL-1 contributed to the increased susceptibility of the *Il1r1-/-* mice, as mice doubly deficient in IL-1R1 and IFNAR1 displayed increased resistance (Mayer-Barber et al., 2014). Our new findings here of increased cytosolic Mtb in *Il1r1-/-* mice provide a possible molecular explanation for the increased type I IFN production previously reported. Future studies need to elucidate the exact mechanisms how IL-1 mediates bacterial containment in phago-lysosomes. In this context, our recent study demonstrated that infected cells themselves do not need to express IL-1R1 *in vivo* to mediate host resistance and that IL-1R1 expression coordinates immune responses in multiple cells

types (Bohrer et al., 2018). Along these lines, it has been proposed that IL-1R1 on non-immune cells was required for the ability of infected alveolar macrophage to leave the airway to establish infection in the interstitial lung space (Cohen et al., 2018). Thus, cytosolic containment of bacilli in infected cells, may not require direct cell-autonomous antimicrobial signaling pathways but may be the result of dynamic cellular interactions between infected cells and cells of both non-hematopoietic and bone marrow origin.

Overall, this study establishes that high level cytosolic escape of mycobacteria can indeed occur *in vivo,* but mainly when host resistance is compromised. When B and T cells are not functional in SCID mice or the complete adaptive immune system is abrogated, like in zebrafish embryos, a substantial percentage of mycobacteria is detected in the cytosol as compared to immunocompetent hosts. Strikingly, the highest proportion cytosolic *Mtb* was observed in mice lacking IL-1 signaling. This argues that the IL-1 pathway is crucial for the control of the number of cytosolic mycobacteria and likely IL-1 mediated resistance to *Mtb*.

Methods

Bacteria

M. marinum E11 strain was grown on Middlebrook 7H10 plates supplemented with OADC. A single colony was inoculated into 7H9 liquid medium (BD) supplemented with 10% ADC and 0.05% Tween 80 and incubated with shaking at 30°C and grown to an OD600 of 0.6-1. Before infection the bacteria were centrifuged at 750 rpm to remove clumps, leaving a bacterial suspension.

Inhibiting acidification

Inhibition of acidification of phagosomes/lysosomes in THP-1 cells treated with Concanamycin B (ConB) (Alexis Biochemicals: 380098C100) was assessed by confocal microscopy. THP-1 macrophages were grown in Roswell Park Memorial Institute (RPMI)-1640 medium

supplemented with 10% FCS and ConB was added to the cells in different concentrations 1h and 24h before fixation. The concentration 10nM of ConB strongly inhibited acidification and did not affect THP-1 cell viability after a 48h incubation period. THP-1 cells were washed 3 times with RPMI-1640 10% FCS medium and kept as a control or pretreated with 10nM ConB for 1 hour. Cells were infected with *M. marinum* (MOI 10:1) in the presence or absence of the acidification inhibitor. After an incubation time of 1 hour at 32°C, cells were washed 3 times with culture medium without antibiotics and with or without acidification inhibitors to remove extracellular bacteria. After washing, the cells were further incubated in culture medium with or without ConB for 24 or 48 hours at 32°C prior to fixation. Fixed samples were prepared for cryo-immunogold microscopy, sectioned for EM and immuno-gold labeled with CD63. To assess the effect on the amount of cytosolic *M. marinum*, from 3 independent experiments, 100-200 randomly chosen bacteria from one grid were counted and for each bacterium it was determined if it was cytosolic or resided in a phago-lysosome.

DAMP assay for measuring lysosomal acidification

Luminal acidification in lysosomes was measured via the probe, DAMP [3-(2,4-dinitroanilino)-3′-amino-N-methyldipropylamine], incubated at 30 µM for 30 min to allow accumulation in acidic compartments. DAMP was quantified by immuno-gold staining using anti-DNP.

Mouse infections

IL1r1$^{-/-}$ mice were purchased from Jackson Laboratories (JAX 3018) and backcrossed to C57BL/6 control mice from Taconic Farms (Hudson, NY) for 11 generations. Male and female mice, 8-12 weeks of age were infected via the aerosol route with *Mtb* H37Rv (100-200 CFU/mouse) as previously described (Bohrer et al., 2018) and sacrificed 27 days later. In short, mice were infected using a whole-body inhalation system (Glas- Col; Terre Haute, IN) exposing the mice to aerosolized *Mtb*. Lungs were perfusion-fixed in 4% paraformaldehyde and 0.4% glutaraldehyde overnight. After fixation, tissues were transferred to storage buffer containing 0.5 % paraformaldehyde. All animals were maintained in an Association for Assessment and

Accreditation of Laboratory Animal Care (AALAC)-accredited BSL2 or BSL3 facilities at the National Institutes of Health (NIH) and experiments performed in compliance with an animal study proposal approved by the National Institute of Immunology Allergy and Infectious Diseases Animal Care and Use Committee.

SCID Mice

Severe combined immunodeficiency (SCID) mice were purchased from Charles River and were aerosol infected with *M. tuberculosis* H37Rv for 21 days, when mice were sacrificed and lungs fixed by perfusion fixation as described below.

BALB/c, B6 mice

Pathogen-free male BALB/c mice, 6-8 weeks old, were anaesthetized with sevoflurane vapours (Abbott Laboratories, Abbott Park, IL, USA) and 100 µl of PBS with 2.5 x 10^5 viable H37Rv bacilli or either Beijing clinical isolates were inoculated intra-tracheally using a stainless steel cannula. Groups of 15 animals were then maintained in cages fitted with microisolators in a BSL-3 biosecurity level facility. Following infection, three mice were euthanized by exsanguination under anesthesia with pentobarbital at days 2, 7, 21, 45 and 120 of infection. Lung tissues were fixed by perfusion fixation as described below.

Zebrafish

Zebrafish embryos and adult zebrafish (Danio rerio) were microinjected with *M. marinum* strain E11 as described by (Weerdenburg et al., 2012) at 30 °C. In short, zebrafish embryos were infected 28h post infection with 100 CFU *M. marinum* wild type through micro-injection in the caudal vein. Adult zebrafish were anaesthetized in 0.02% MS-222 (Sigma) and injected intra-peritoneally with 2x10^4 *M. marinum* Tn::ESX-5. The embryos were incubated for 6 or 9 days and fixed as described below. For classification of the subcellular localization, 3 embryos of 9 days incubation were used. Three adult fish were infected with E11 or E11 ESX5 mutant (Weerdenburg et al., 2012) and sacrificed at day 11 when the spleen was dissected out and fixed as described below.

Armadillo

Male Armadillos were intradermally inoculated in the abdomen with either 1 x 10^7 live or irradiated *M. leprae* (0.1 ml). After, 3, 11 and 21 days post-inoculation, 6 mm punch biopsies were taken from the boarder of the depigmented area at the inoculation sites and fixed for 2 hours as described below. For classification of the subcellular localization, 1-2 punches were used from day 3 and day 21. As no lysosomal markers suited for immuno-TEM analysis were known, anti-Cell Wall Protein (CWP) was used to immuno-label the leprosy bacteria.

Human samples

Leprosy skin biopsies were taken at the boarder of the depigmented lesions with written consent from 4 different lepromatous leprosy patients. Materials were directly incubated in EM grade fixatives and transported to the EM lab in fixatives.

Fixation of tissues

All tissues were fixed in a combination of 4% paraformaldehyde and 0.4% glutaraldehyde in 0.2M PHEM (with 240mM PIPES, 100mM HEPES, 8mM MgCl2 and 40mM EGTA) buffer. Fixation for at least 2 hours in fixative containing glutaraldehyde is essential to kill mycobacteria. After fixation, tissues were transferred to storage buffer containing 0.5 % paraformaldehyde in 0.2M PHEM buffer.

Embedding and sectioning

After fixation, tissues were washed in phosphate buffered saline (PBS), to remove fixatives. The required structures were dissected out using a razor blade and cut into 1-3 mm^2 sized blocks. Lung tissue was embedded in increasing percentages gelatin (2%, 5% and 12% in 0.1M phosphate buffer) and incubated at 37 °C. After the removal from liquid gelatin, blocks were incubated overnight in 2.3M sucrose at 4 °C. Then blocks were snap frozen and stored in liquid nitrogen till sectioned. After trimming at -100 °C, semi thin sectioning was performed for analysis with fluorescence microscopy or ultra-thin sectioning at -120 °C was performed

using a diamond Diatome cryo-immuno knife on a Leica Ultracut UC6. Sections are picked up with a loop filled with a 1:1 mixture of 2,3 M sucrose and 1% tylose (Metylcellulose, G1095) in milliQ water and placed on a copper, formvar coated grid or glass slides. Grids with sections were stored at 4 °C till immuno-labeled. Fluorescence Microscopy was used to search the region of infection as described in van Leeuwen et al., 2018 and van der Wel et al., 2005. In short, semi-thin sections (200-300nm) of the whole sample were labelled with Hoechst 33342 (Thermo Fisher) to indicate the nuclei of the tissue and anti-Cell Wall protein labelling was used to indicate mycobacteria.

Immuno-gold labelling

Grids with cryo-sections were incubated on 2% gelatin in 0.1M phosphate buffer plates at 37 °C for 30 min. Thereafter, grids were washed with PBS/0.02M glycine, blocked with 1% BSA and incubated for 45 minutes with primary antibody. Various antibodies were used on different tissues: for human skin and sputum: Cathapsin-B (Zymed, clone 1C11), Lysosome Associated Membrane Protein 1 and 2 (LAMP1 and LAMP2) (Pharmingen, H4A3 and H4B3), Cluster of Differentiation CD63 (clone 435 Sanquin). For Zebrafish anti-actin (Sigma AC-15), and tested but without specific labeling: anti-LAMP (Pharmingen, H4A3 and H4B3, Abcam ab67283), anti CD63 (clone 435 Sanquin). For *M. leprae*, anti Cell Wall Protein (C188, a kind gift form John Spencer and Patrick Brennan Colorado State University). DAMP (N-(3-((2,4-Dinitrophenyl) Amino)propyl)-N-(3-Aminopropyl) Methylamine, Dihydrochloride) detection was performed using anti dinitrophenol (DNP) (Polyclonal Anti-DNP, Oxford Biomedical Research). All antibodies were diluted in 1% BSA in PBS. After washing in PBS/0.02M glycine and blocking in 0.1% BSA in PBS/0.02M glycine, grids are incubated on bridging antibody when primary antibody was monoclonal or goat origin. After washing and blocking, grids are incubated on protein A gold diluted in 1% BSA in PBS. To remove unbound gold, grids were washed with PBS and fixed using 1% glutaraldehyde in PBS, then washed with MiliQ and contrasted with uranyl acetate and methylcellulose at pH 4.

Immuno-fluorescence labelling

Semi-thin sections (200-300nm) placed on glass were washed with PBS/0.02M Glycine and incubated with primary antibody anti Cell Wall Protein for 45 minutes. Then, the sections were washed with PBS and incubated with secondary antibody goat-anti-rabbit Alexa 488 (Mol. Probes, A32731) for 20 minutes and Hoechst 33342 for 5 minutes (Thermo Fisher, H3570). After washing with PBS, samples were mounted with Vectashield. The sections were imaged using a Leica DM6 wide-field microscope and images were analyzed using FIJI.

Statistical analysis and subcellular classification

Statistical analysis was performed using Graphpad-Prism 8.0 software. In the legends, the average is given with the standard deviation and n indicate the number of bacteria localized in a specific subcellular compartment. Significance was determined by using unpaired T test and defined in the graphs as $P<0.05$ = *, $P<0.01$ = ** and $P<0.001$ = ***. The number of biological samples, and bacteria counted in mice are listed in Supplemental Table 1.

Classification of the subcellular localization of bacteria was performed blindfolded and by 2 individual counters to establish inter-counter reproducibility. Bacteria are classified as cytosolic when 1/3 or less of the bacteria or bacterial cluster is surrounded by a visible membrane and 2 or less gold particles detecting lysosomal markers are present. Bacteria are classified as phagosomal when 1/3 or more of the bacteria or bacterial cluster is surrounded by a visible membrane and 2 or less gold particles detecting lysosomal markers is present and phago-lysosomal when 1/3 or more of the bacteria or bacterial cluster is surrounded by a visible membrane and 3 or more gold particles detecting lysosomal markers are present.

Ethics statement

SCID mouse infections were performed in agreement with European and French guidelines (Directive 86/609/CEE and Decree 87–848 of 19 October 1987). The experiments received the approval by the Institut Pasteur Safety Committee (Protocol 11.245) and the ethical

approval by local ethical committees “Comité National de Réflexion Ethique sur l’Expérimentation Animale N° 59 (CNREEA)”.

Adult zebrafish of the local Free University of Amsterdam (VU) line were handled in compliance with the local animal welfare regulations and approved by the local animal welfare commission (IvD) of the VU/Amsterdam University Medical Centre. For zebrafish embryo experiments that are performed within the grace period (i.e. first 6 days) no special permission is allowed, since these experiments fall under animal experimentation law according to the EU Animal Protection Directive 2010/63/EU.

BALB/c mouse infections were approved by the Institutional Ethics Committee of Animals Experimentation of the National Institute of Medical Sciences and Nutrition Salvador Zubirán in accordance with the guidelines of the Mexican national regulations on Animal Care and Experimentation NOM 062-ZOO-1999

Experiments using armadillos were performed in accordance with USPHS Policy on the Humane Care and Use of Laboratory Animals and the USDA Animal and Plant Health Inspection Service. The Institutional Animal Care and Use Committee reviewed and approved the protocol.

Acknowledgements

We would like to thank Wikky Tigchelaar – Gutter, Pekka Kujala, Hans Janssen for EM analysis, Gidado Mustapha, Nigeria for leprosy skin biopsies and Peter Peters for facilitating EM analysis and starting the project. We are also grateful to Wafa Frigui and Alexandre Pawlik for help with infection experiments. We would like to thank Branch Moody for critically reading the manuscript and the helpful comments. RB acknowledges support by ANR-10-LABX-62-IBEID. SvdN and NvdW acknowledge NIH grant no AI116604 and Netherlands Leprosy Relief. The NIH, NIAID funded the armadillo studies through the Interagency Agreement No. AAI15006 with the Health Resources and Services Administration, Healthcare Systems Bureau, National Hansen’s Disease Program.

Author contributions

SvdN, ER, KDMB and NvdW wrote the manuscript, SvdN, MvZ, KdP, AG, SR, SM, DH performed EM analysis AvdS, WB, RB, RHP, MP performed infection experiments, KDMB performed and designed experiments and NvdW conceived and designed experiments.

Declaration of interests

The authors declare no competing interests.

535 **Main Figure titles + Legends**

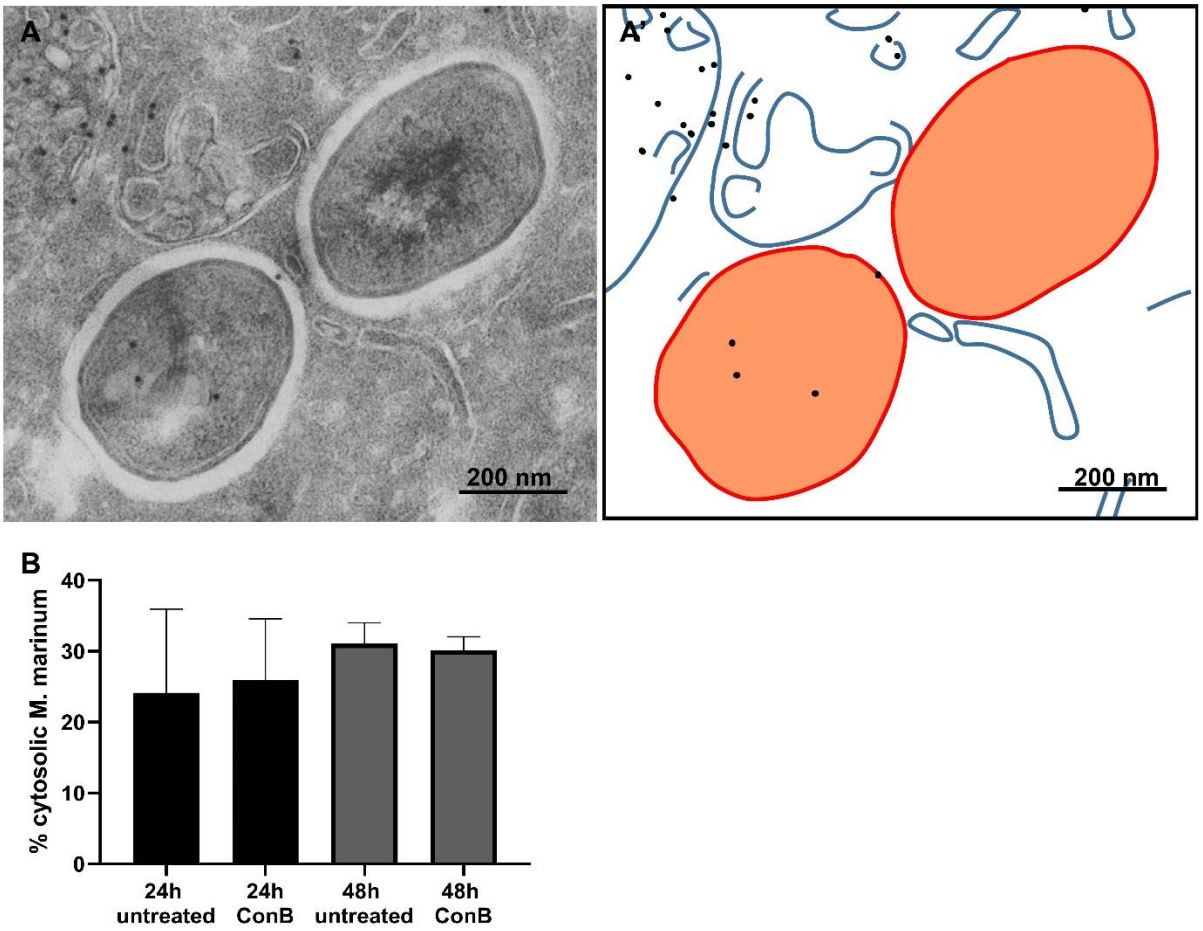

536

537 **Legend Figure 1. The pH of the phago-lysosome does not affect cytosolic translocation**
538 **of *M. marinum*.** A) Electron micrograph of a THP-1 cell infected with *M. marinum* for 24 hour
539 in the presence of ConB showing *M. marinum* in the cytosol without membrane and CD63
540 labeling. CD63 immunolabelling indicated by 10 nm gold particles is present on the
541 multivesicular lysosome in the left top corner. A') schematic representation of micrograph in A
542 with in blue lines host membranes, black dots CD63 labelling indicated by 10 nm gold particles,
543 orange bacteria and bar represents 200 nm. B) Quantification of the percentage of *M. marinum*
544 in the cytosol 24 and 48 hours after infection using immuno-gold labelling for CD63 (see also
545 supplemental Figure 2A). Cells were treated with ConB to raise lysosomal pH, which did not
546 affect the percentage of cytosolic *M. marinum*. Error bars represent the standard deviation of
547 3 experiments.

548 **Figure 2**

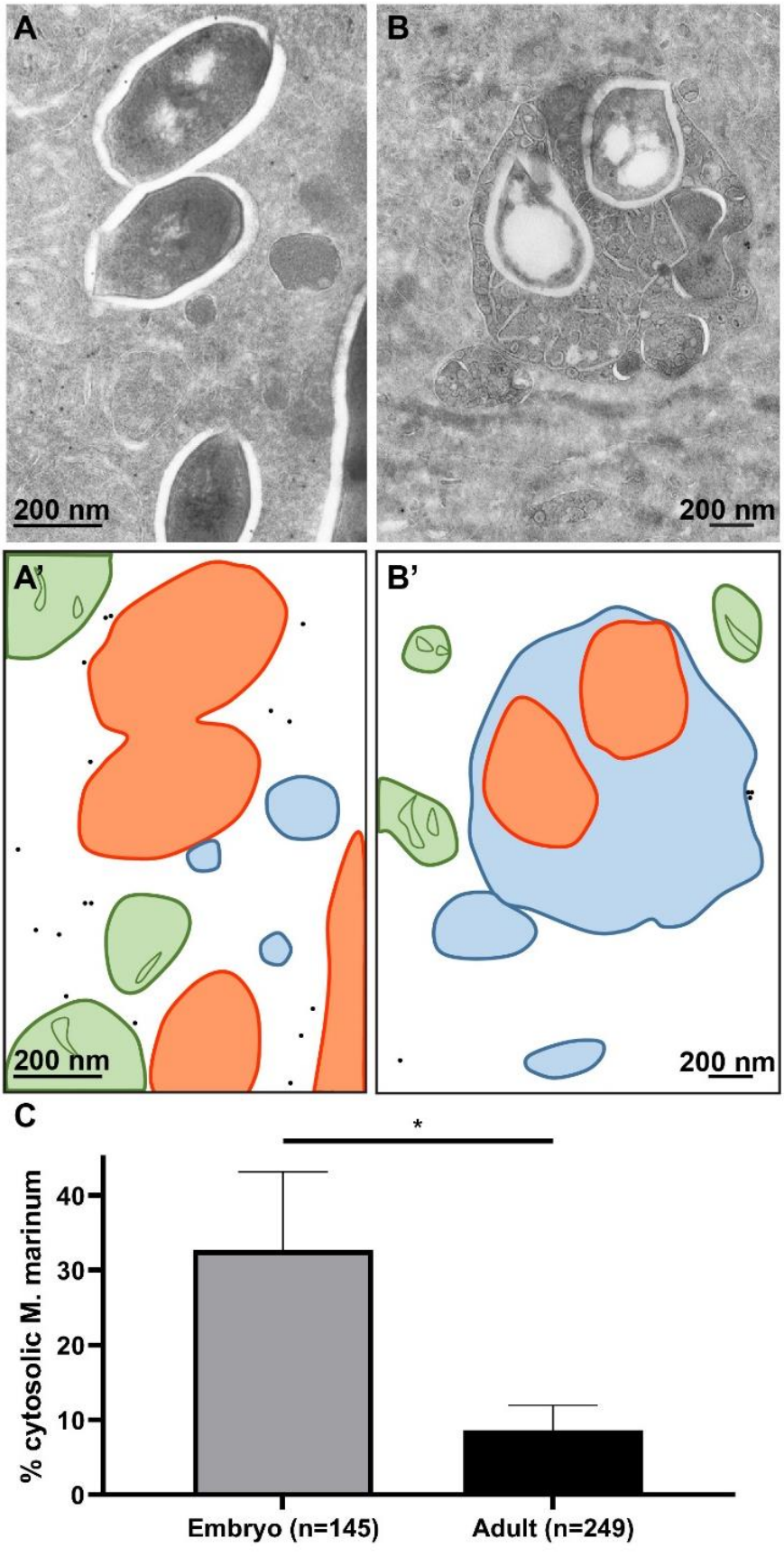

549

Legend Figure 2: Cytosolic localization of *M. marinum* in zebrafish is abundant when the adaptive immune system is yet developed. Embryo and adult zebrafish infected with *M. marinum* were analysed using TEM. A) Cytosolic *M. marinum* in zebrafish embryo tissue. B) Phagosomal *M. marinum* ΔESX5 in adult zebrafish tissue. A') and B') Schematic representation of A and B, with black dots indicating actin immuno-gold labelling, orange lines *M. marinum* and blue lines phagosomal and host membranes, green lines mitochondria. C) Quantification of the percentage of cytosolic *M. marinum* at embryo day 9 and in spleen adult zebrafish at day 11 (see also Supplemental Figure 2B). Error bars indicate standard deviation between 3 different zebrafish embryos and 3 adult fish, n represents the total number of bacteria counted.

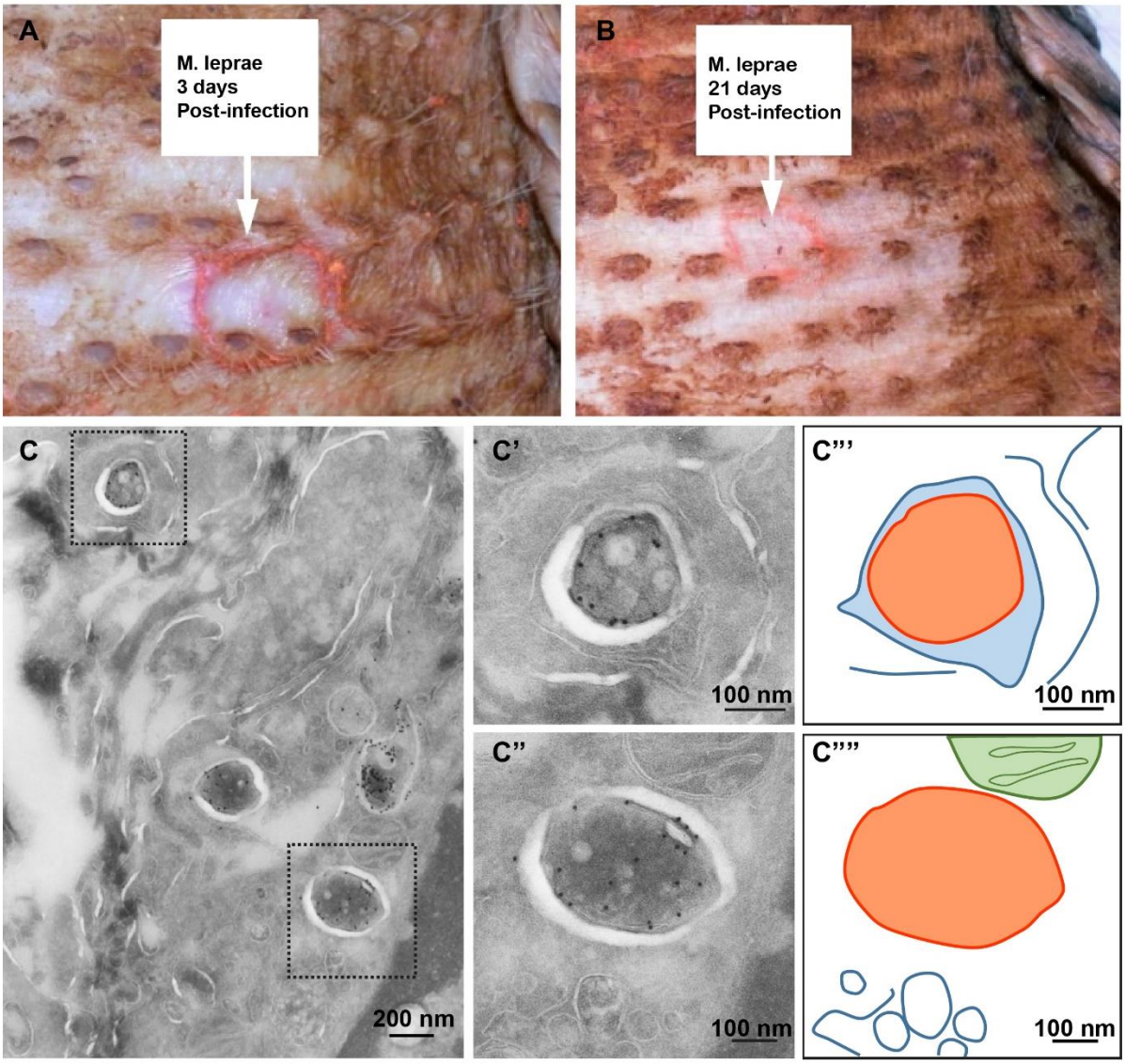

Legend Figure 3: Restrained cytosolic *M. leprae* localization in armadillo skin biopsies. Live *M. leprae* injected in the skin of the armadillo at the red circle indicated by the white arrow text box. The skin was observed at A) 3 days after infection and B) 21 days after infection. At infection sites loss of pigmentation was detected. C) TEM image of infected armadillo skin biopsy 3 days after infection with viable *M. leprae*. Immuno-gold labelling using αCWP to indicate *M. leprae*. C') enlargement of boxed area in C, *M. leprae* enclosed by host membranes and thus phagosomal. C"), enlargement of lower boxed area in C, *M. leprae* was not enclosed by host membranes and thus cytosolic. C'"), C'"') Schematic representation of C' and C" with in orange *M. leprae* and the blue lines indicate host membranes and green mitochondrial membranes. Total number of bacteria detected at day 3 is 47 and at day 21 is 45.

571 **Figure 4.**

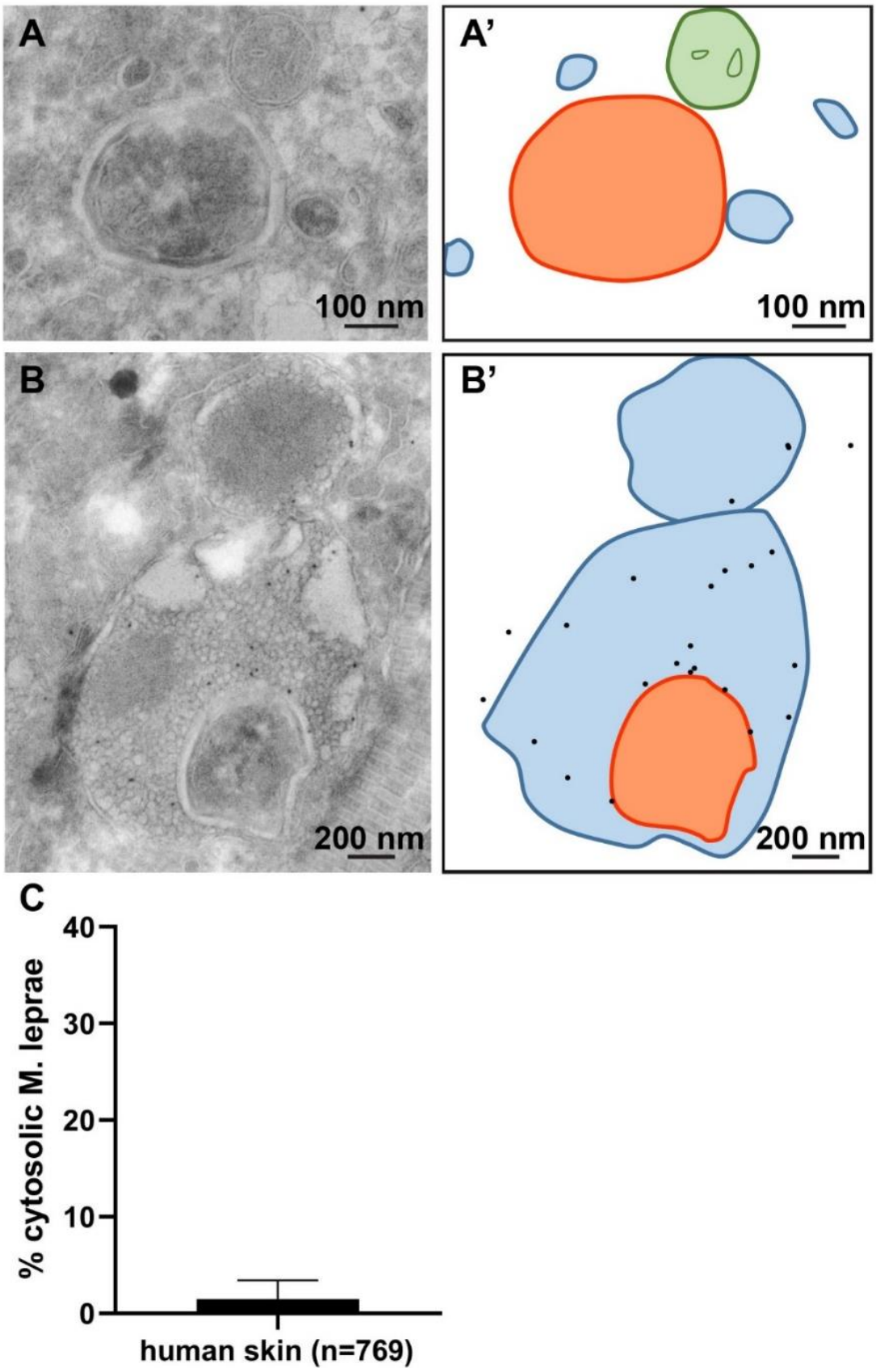

572

573

574 **Legend Figure 4. Restrained cytosolic localization of *M. leprae* in human skin biopsies.**
575 Leprosy patient skin biopsies were analyzed using TEM. Immuno-gold labelling for Cathepsin-
576 D was used to label lysosomes and phagolysosomes. A) TEM image of patient skin biopsy
577 with cytosolic *M. leprae*, the mycobacteria was not enclosed with host membranes. A')
578 Schematic representation of A, orange indicate *M. leprae,* blue lines indicate host membranes,
579 and green mitochondria. B) *M. leprae* present in the phagolysosome, the mycobacterium is
580 enclosed by host membranes, immunogold labelled for lysosomal marker Cathepsin-D. B')
581 Schematic representation of B, black dots indicate Cathepsin-D labelling, orange indicate *M.*
582 *leprae* and the blue lines indicate phagolysosomal membranes. C) Quantification of the
583 average percentage of *M. leprae* present in the cytosol, error bar indicates standard deviation
584 from 4 different patients, n represents the total number of intracellular bacteria (see also
585 Supplemental Figure 2C).

586 **Figure 5.**

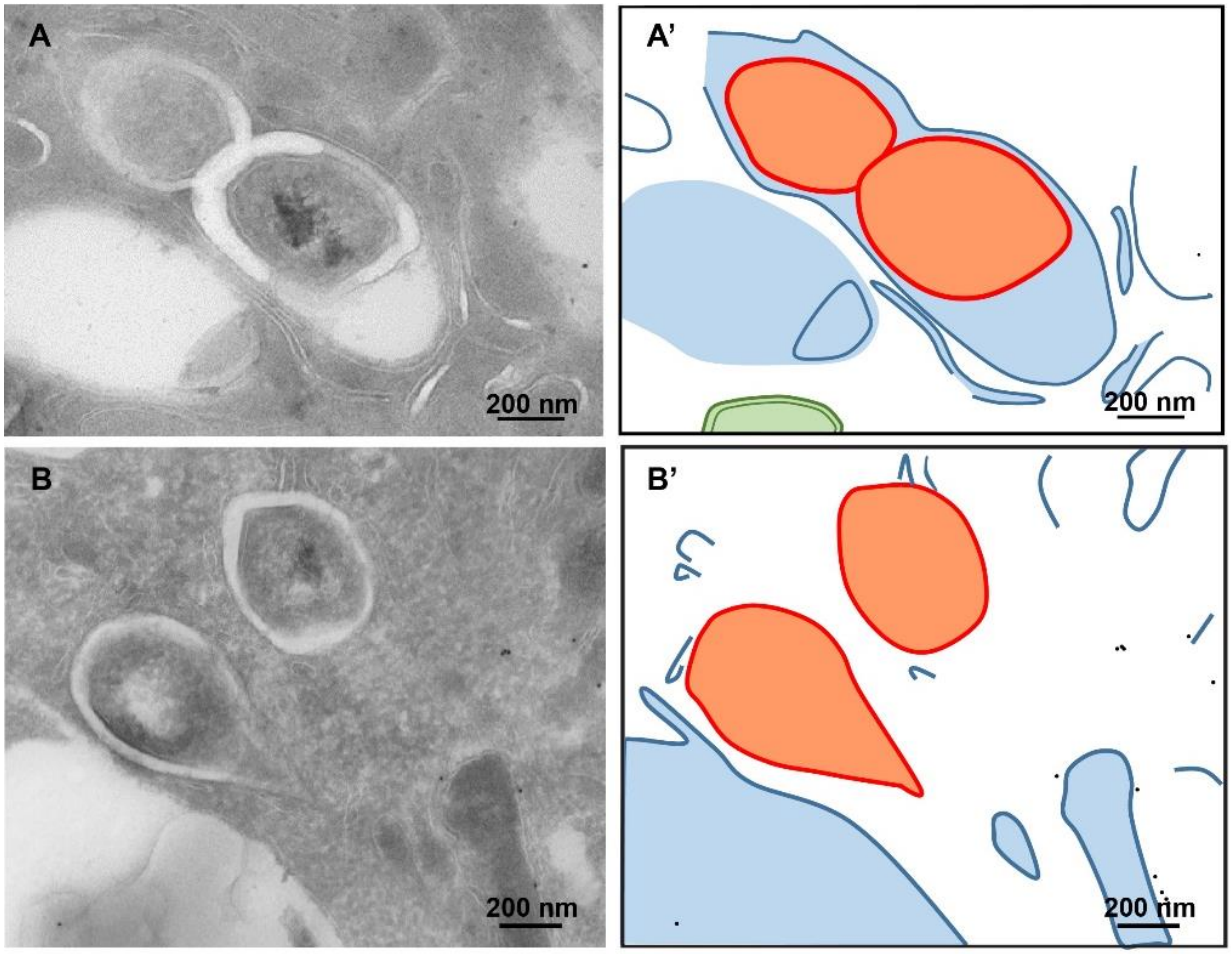

587

588

589 **Legend Figure 5. Early cytosolic localization of *Mtb* in SCID mouse lungs.** A,B) Sections
590 of SCID mice lung tissue infected with *Mtb* H37Rv for 21 days were labelled for LAMP1 using
591 immuno-gold labelling, to indicate lysosomes. A'B') schematic representation with in orange
592 *Mtb*, blue lines host membranes, black dots gold particles indicating LAMP1 decorated
593 lysosomes and green mitochondria. A) cross section of *Mtb* surrounded by cellular membranes
594 thus phagosomal. B) *Mtb* is present in the cytosol, without cellular membranes surrounding the
595 bacteria, scale bar indicates 200 nm. Information number of imaged bacteria and mice see
596 Supplemental Table 1.

Figure 6.

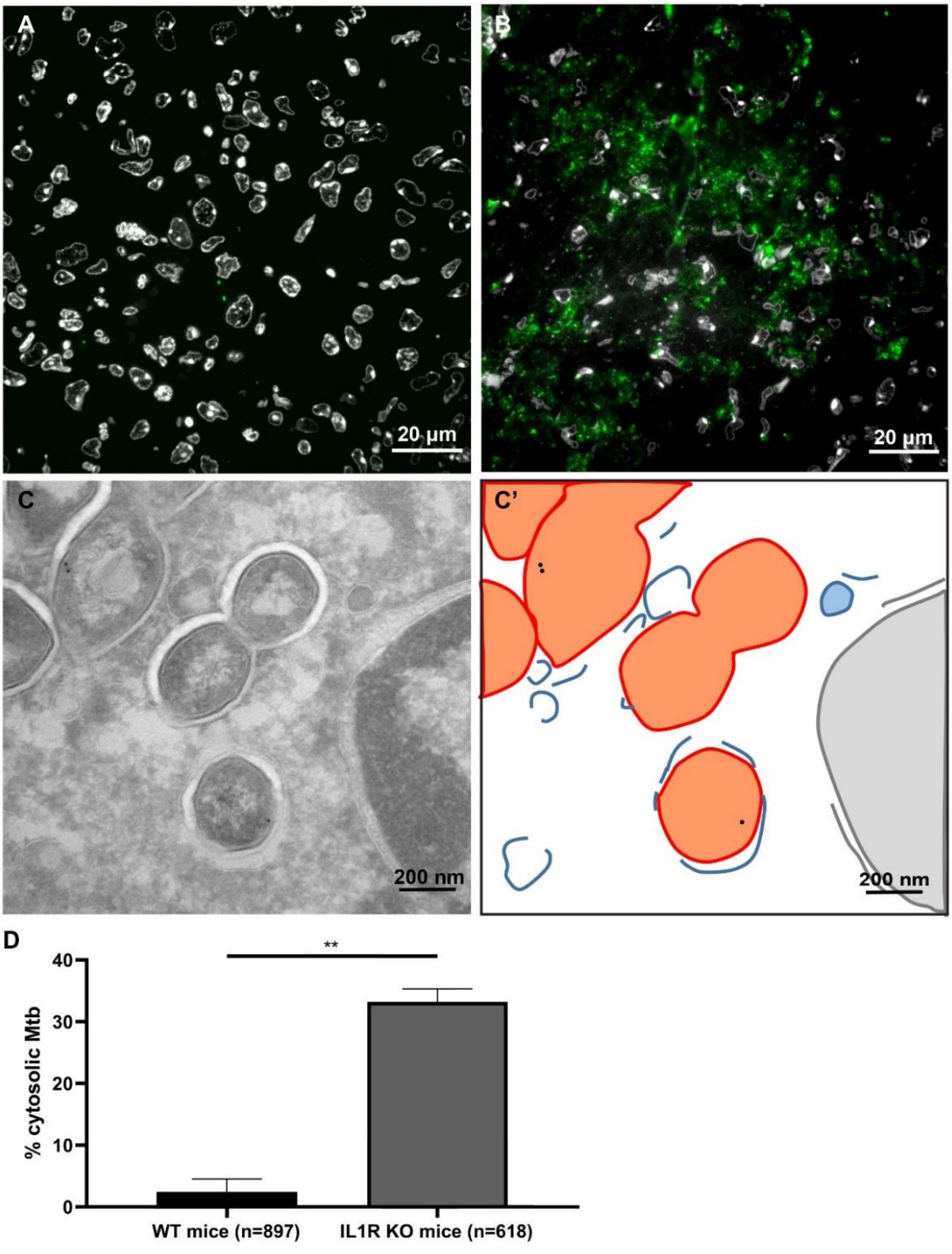

599 **Legend Figure 6. *Mtb* preferentially localize to the cytosol in *Il1r1-/-* mice.** Fluorescence
600 microscopy of 200 nm sections stained with DAPI for nuclei (white) and anti-cell wall protein
601 to detect *Mtb* (green) in granuloma in lung tissue of A) WT B6 mice and B) *Il1r1-/-* mice infected
602 with *Mtb* for 28 days. C) Immuno-gold labelling using LAMP1 indicate lysosomal membranes
603 in *Il1r1-/-* mice imaged using TEM. C') schematic representation of C, *Mtb* is depicted in
604 orange, host membranes in blue and host nucleus in pink. D) Quantification of the localization
605 of *Mtb* in B6 and *Il1r1-/-* lungs, here presenting cytosolic localization (see also Supplemental
606 Figure 2D). Error bars indicate standard deviation based on the analysis of 897 (WT) or 618
607 (*Il1r1-/-*) bacteria in multiple granulomas of 2 WT B6 and 2 *Il1r1-/-* mice.

608 **Supplemental items titles and legends van der Niet et al.,**

609 **Supplemental Figure 1**

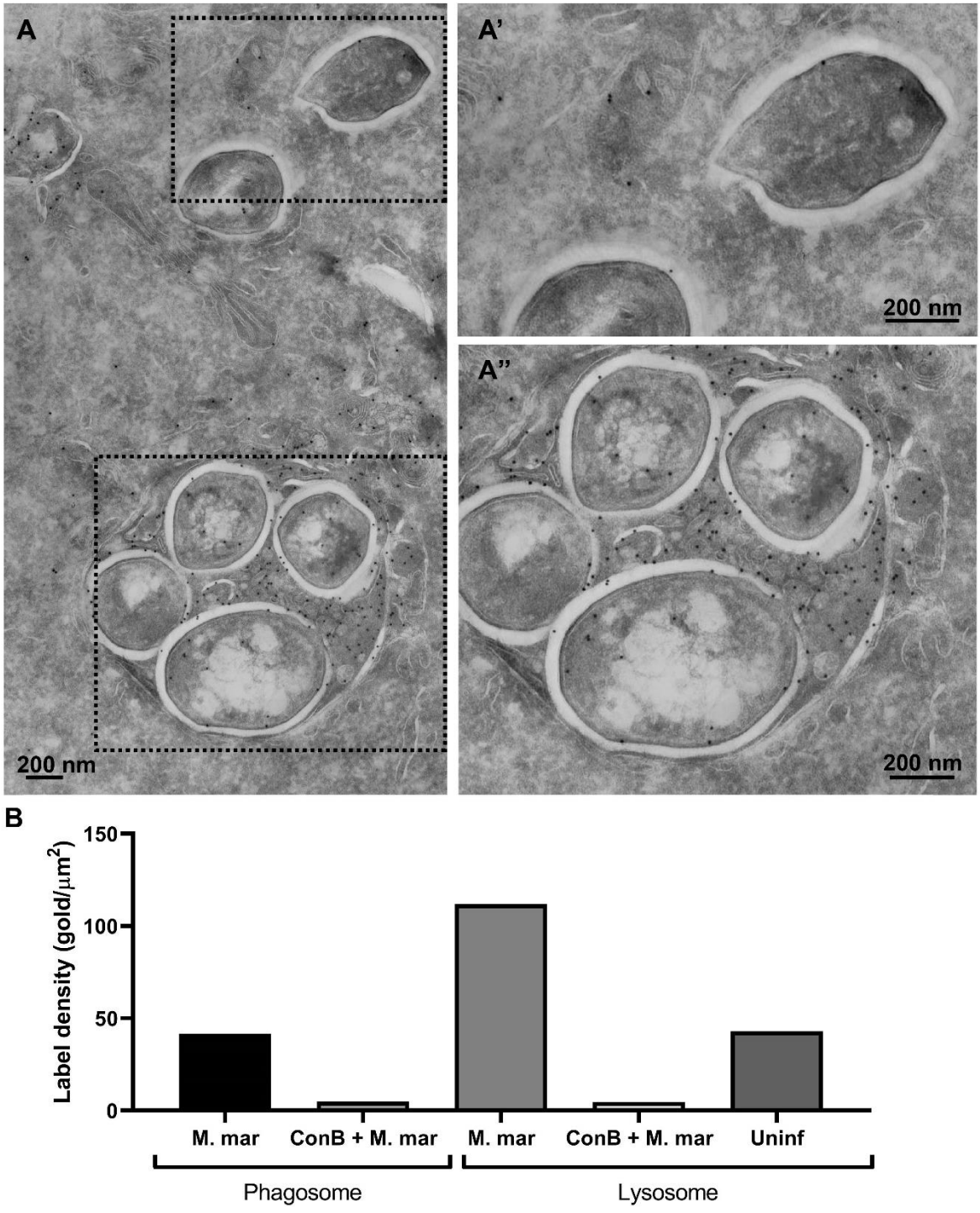

610

Legend Supplemental Figure 1:

The pH of the phago-lysosome does not affect cytosolic translocation of *M. marinum*. A) *M. marinum* infected THP-1 cells were incubated with DAMP to identify acidic organelles. Thereafter, the cells were fixed and analyzed using TEM. The acidity of the lysosome was determined using immuno-gold labelling against DAMP using DNP, the higher the label density the more acidic the phagosome or lysosome. A') cytosolic *M. marinum* without membranes enclosing the mycobacteria. A") Lysosomal *M. marinum*, enclosed by host membrane and DAMP labelled. B) Label density as measured in the number of gold particles per μm^2 on *M. marinum* containing phagosomes or lysosomes in *M. marinum* infected THP-1 cells, *M. marinum* infected Con B treated THP-1 cells and uninfected untreated THP-1 cells.

621 **Supplemental Figure 2**

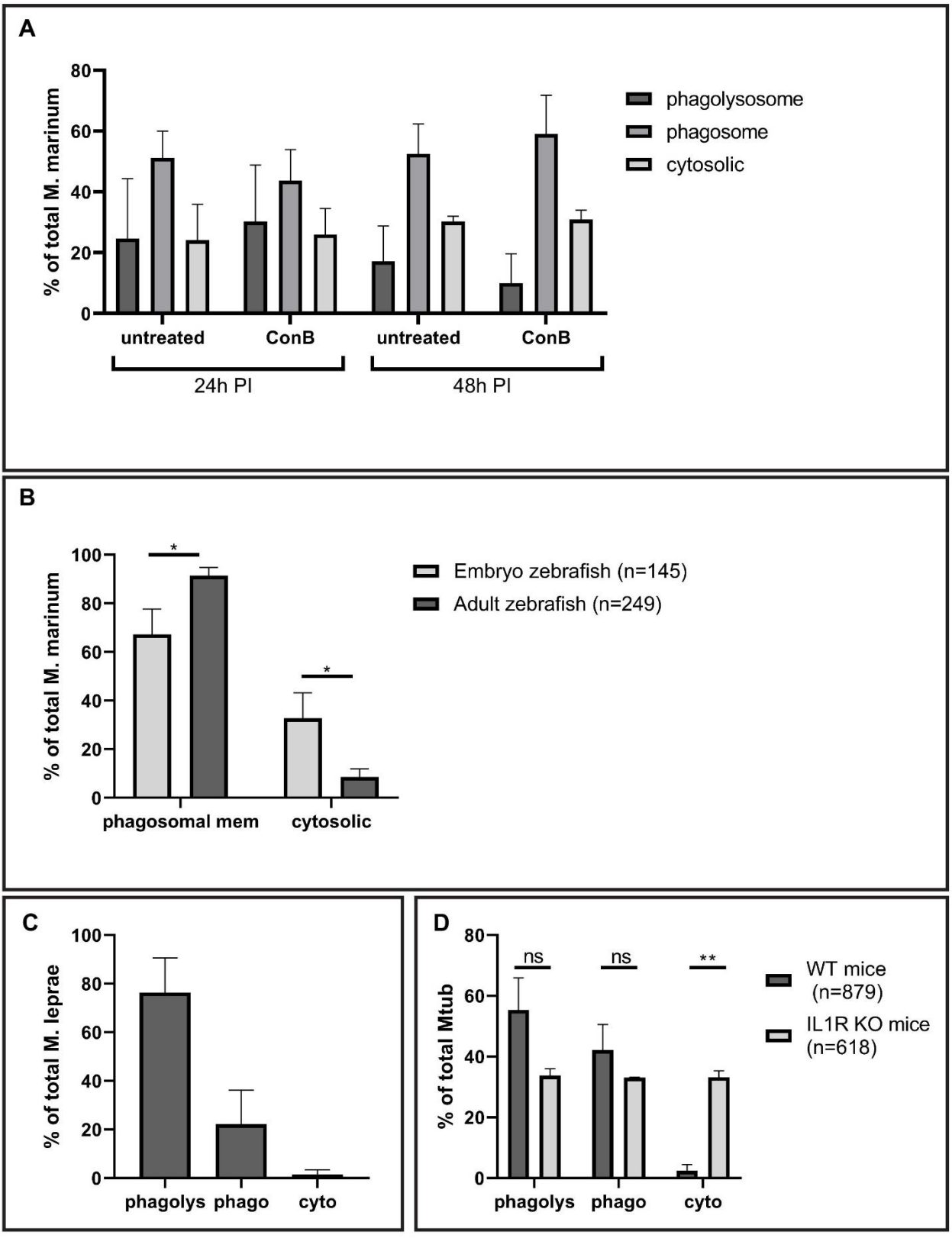

622

Legend Supplemental Figure 2

Quantification of the percentage of mycobacteria in the phagosome, phagolysosome or cytosol using immuno-gold labelling and TEM analysis. The bacteria are classified as phagolysosomal when a host membrane is immunogold labelled with at least 2 gold conjugated to lysosomal markers such as CD63, LAMP1 or Cathepsin D are present, phagosomal with less than 2 gold marked membrane enclosed compartment are present and cytosolic when both membrane and gold is absent.

A) Subcellular localization *M. marinum* in THP1 cells treated with ConB or untreated. Immunogold labelling with CD63 average of 3 experiments with 100-200 bacteria classified (Related to Figure 1B).

B) Subcellular localization *M. marinum* in zebrafish embryo day 9 and in spleen adult zebrafish day 11, error bars indicate standard deviation between 3 different zebrafish embryos and 3 adult fish. In three embryonic zebrafish, 17, 54 and 74 bacteria were detected and in three adult zebrafish 91, 8 and 150 bacteria were detected and catagorized. As no good lysosomal markers are present, a discrimination between phagolysosomal and phagosomal can not be made (Related to Figure 2C).

C) Subcellular localization of *M. leprae* in skin biopsies of 4 different leprosy patients, using Cathepsin-D as a lysosomal marker, error bar indicates standard deviation from 4 different patients, where respectively 165, 248, 49 and 307 individual bacteria were detected and classified for their subcellular localization (Related to Figure 4C).

D) Subcellular localization of *Mtb* in lung of WT B6 mice and *Il1r1-/-* mice 4 weeks infected using LAMP1 as a lysosomal marker (Related to Figure 6D). Error bars represent standard deviation based on the analysis of 897 (WT) or 618 (*Il1r1-/-*) bacteria in multiple granulomas of 2 WT B6 and 2 *Il1r1-/-* mice (Related to Figure 6).

647 **Supplemental Table 1**

Mouse	Mtb strain	Day of infection	% bacteria in phago-lysosome	% bacteria in phagosome	% bacteria in cytosol	n counted bacteria	n mice
BALB/c	H37Rv	D2	38	62	0	47	1
		D7	71	23	6	52	2
		D21	0.4	98	2	247	2
		D45	0	100	0	5	1
		D120	0	97	3	38	2
	1998-1500 Ancient Beijing	D21	0	93	7	31	1
		D45	0	100	0	193	1
		D120	0	100	0	35	2
	2002-0230 Beijing	D120	0	100	0	166	2
SCID	H37Rv	D21	29	54	17	167	1

648

649 **Legend Supplemental Table 1:**

650 Overview of the subcellular localization of various *Mtb* strains infected at different days of
651 infection in BALB/c or SCID mice. The number of bacteria used and the number of mice in
652 which bacteria were detected are given in the last 2 columns. Similar to Supplemental figure
653 1, bacteria are classified as phagolysosomal, phagosomal or cytosolic based on the number
654 of gold attached to lysosomal markers and the presence of a membrane.

References

Armstrong, J. A., & D'Arcy Hart, P. (1971). Response of cultured macrophages to mycobacterium tuberculosis, with observations on fusion of lysosomes with phagosomes. *J Exp Med*, *134*(3), 713–740.

Augenstreich, J., Arbues, A., Simeone, R., Haanappel, E., Wegener, A., Sayes, F., … Astarie-Dequeker, C. (2017). ESX-1 and phthiocerol dimycocerosates of Mycobacterium tuberculosis act in concert to cause phagosomal rupture and host cell apoptosis. *Cellular Microbiology*, *19*(7), 1–19. https://doi.org/10.1111/cmi.12726

Bohrer, A. C., Tocheny, C., Assmann, M., Ganusov, V. V., & Mayer–Barber, K. D. (2018). Cutting Edge: IL-1R1 Mediates Host Resistance to Mycobacterium tuberculosis by Trans -Protection of Infected Cells . *The Journal of Immunology*, *201*(6), 1645–1650. https://doi.org/10.4049/jimmunol.1800438

Buter, J., Cheng, T.-Y., Ghanem, M., Grootemaat, A. E., Raman, S., Feng, X., … Moody, D. B. (2019). Mycobacterium tuberculosis releases an antacid that remodels phagosomes. *Nature Chemical Biology*, *15*(9), 889–899. https://doi.org/10.1038/s41589-019-0336-0

Chen, Q., Sun, L., & Chen, Z. J. (2016). Regulation and function of the cGAS-STING pathway of cytosolic DNA sensing. *Nature Immunology*, *17*(10), 1142–1149. https://doi.org/10.1038/ni.3558

Clemens, D. L., Lee, B. Y., & Horwitz, M. A. (2000). Mycobacterium tuberculosis and Legionella pneumophila phagosomes exhibit arrested maturation despite acquisition of Rab7. *Infection and Immunity*, *68*(9), 5154–5166. https://doi.org/10.1128/IAI.68.9.5154-5166.2000

Cohen, S. B., Gern, B. H., Delahaye, J. L., Adams, K. N., Plumlee, C. R., Winkler, J. K., … Urdahl, K. B. (2018). Alveolar Macrophages Provide an Early Mycobacterium tuberculosis Niche and Initiate Dissemination. *Cell Host and Microbe*, *24*(3), 439-

446.e4. https://doi.org/10.1016/j.chom.2018.08.001

Collins, A. C., Cai, H., Li, T., Franco, L. H., Li, X. D., Nair, V. R., … Shiloh, M. U. (2015). Cyclic GMP-AMP Synthase Is an Innate Immune DNA Sensor for Mycobacterium tuberculosis. *Cell Host and Microbe*, *17*(6), 820–828. https://doi.org/10.1016/j.chom.2015.05.005

Crowle, A. J., Dahl, R., Ross, E., & May, M. H. (1991). Evidence that vesicles containing living, virulent Mycobacterium tuberculosis or Mycobacterium avium in cultured human macrophages are not acidic. *Infection and Immunity*, *59*(5), 1823–1831.

Doitsh, G., & Greene, W. C. (2016). Dissecting how CD4 T cells are lost during HIV infection. *Cell Host and Microbe*, *19*(3), 280–291. https://doi.org/10.1016/j.physbeh.2017.03.040

Dupuis, S., Döffinger, R., Picard, C., Fieschi, C., Altare, F., Jouanguy, E., … Casanova, J. L. (2000). Human interferon-g-mediated immunity is a genetically controlled continuous trait that determines the outcome of mycobacterial invasion. *Immunological Reviews*, *178*, 129–137.

Flynn, J. A. L., Chan, J., Triebold, K. J., Dalton, D. K., Stewart, T. A., & Bloom, B. R. (1993). An essential role for interferon γ in resistance to mycobacterium tuberculosis infection. *Journal of Experimental Medicine*, *178*(6), 2249–2254. https://doi.org/10.1084/jem.178.6.2249

Gröschel, M. I., Sayes, F., Shin, S. J., Frigui, W., Pawlik, A., Orgeur, M., … Brosch, R. (2017). Recombinant BCG Expressing ESX-1 of Mycobacterium marinum Combines Low Virulence with Cytosolic Immune Signaling and Improved TB Protection. *Cell Reports*, *18*(11), 2752–2765. https://doi.org/10.1016/j.celrep.2017.02.057

Guirado, E., Mbawuike, U., Keiser, T. L., Arcos, J., Azad, A. K., Wang, S. H., & Schlesinger, L. S. (2015). Characterization of host and microbial determinants in individuals with latent tuberculosis infection using a human granuloma model. *MBio*, *6*(1), 1–13.

https://doi.org/10.1128/mBio.02537-14

Houben, D., Demangel, C., van Ingen, J., Perez, J., Baldeón, L., Abdallah, A. M., … Peters, P. J. (2012). ESX-1-mediated translocation to the cytosol controls virulence of mycobacteria. *Cellular Microbiology*, *14*(8), 1287–1298. https://doi.org/10.1111/j.1462-5822.2012.01799.x

Huang, L., Nazarova, E. V., Tan, S., Liu, Y., & Russell, D. G. (2018). Growth of Mycobacterium tuberculosis in vivo segregates with host macrophage metabolism and ontogeny. *Journal of Experimental Medicine*, *215*(4), 1135–1152. https://doi.org/10.1084/jem.20172020

Ji, D. X., Yamashiro, L. H., Chen, K. J., Mukaida, N., Kramnik, I., Darwin, K. H., & Vance, R. E. (2019). Type I interferon-driven susceptibility to Mycobacterium tuberculosis is mediated by interleuking-1 receptor antagonist IL-1Ra. *Nature Microbiology*, *4*(12), 2128–2135. https://doi.org/10.1016/j.physbeh.2017.03.040

Juffermans, N. P., Florquin, S., Camoglio, L., Verbon, A., Kolk, A. H., Speelman, P., & Deventer, S. J. H. Van. (2000). Interleukin-1 Signaling Is Essential for Host Defense during Murine Pulmonary Tuberculosis. *The Journal of Infectious Diseases*, 902–908.

Kupz, A., Zedler, U., Stäber, M., Perdomo, C., Dorhoi, A., Brosch, R., & Kaufmann, S. H. E. (2016). ESAT-6 – dependent cytosolic pattern recognition drives noncognate tuberculosis control in vivo. *The Journal of Clinical Investigation*, *126*(6), 2109–2122. https://doi.org/10.1172/JCI84978DS1

Langenau, D. M., Ferrando, A. A., Traver, D., Kutok, J. L., Hezel, J. D., Kanki, J. P., … Trede, N. S. (2004). In vivo tracking of T cell development , ablation , and engraftment in transgenic zebrafish. *PNAS*, *101*(19), 7369–7374.

Leake, E. S., Myrvik, Q. N., Wright, M. J., & Carolina, N. (1984). Phagosomal Membranes of Mycobacterium bovis BCG-Immune Alveolar Macrophages Are Resistant to Disruption

730 by Mycobacterium tuberculosis H37Rv. *Infection and Immunity*, *45*(2), 443–446.

731 Lerner, T. R., Borel, S., & Gutierrez, M. G. (2015). The innate immune response in human
732 tuberculosis. *Cellular Microbiology*, *17*(9), 1277–1285. https://doi.org/10.1111/cmi.12480

733 Lerner, T. R., Carvalho-Wodarz, C. D. S., Repnik, U., Russell, M. R. G., Borel, S., DIedrich,
734 C. R., … Gutierrez, M. G. (2016). Lymphatic endothelial cells are a replicative niche for
735 Mycobacterium tuberculosis. *Journal of Clinical Investigation*, *126*(3), 1093–1108.
736 https://doi.org/10.1172/JCI83379

737 Lerner, T. R., Queval, C. J., Fearns, A., Repnik, U., Griffiths, G., & Gutierrez, M. G. (2018).
738 Phthiocerol dimycocerosates promote access to the cytosol and intracellular burden of
739 Mycobacterium tuberculosis in lymphatic endothelial cells. *BMC Biology*, 1–13.
740 https://doi.org/10.1186/s12915-017-0471-6

741 Lerner, T. R., Queval, C. J., Lai, R. P., Russell, M., Fearns, A., Greenwood, D. J., …
742 Gutierrez, M. G. (2020). Mycobacterium tuberculosis cords in the cytosol of live
743 lymphatic endothelial cells to evade host immune surveillance. *JCI Insight*.

744 Majlessi, L., & Brosch, R. (2015). Mycobacterium tuberculosis Meets the Cytosol: The Role
745 of cGAS in Anti-mycobacterial Immunity. *Cell Host and Microbe*, *17*(6), 733–735.
746 https://doi.org/10.1016/j.chom.2015.05.017

747 Marino, S., Pawar, S., Fuller, C. L., Reinhart, T. A., Flynn, J. L., & Kirschner, D. E. (2004).
748 Dendritic Cell Trafficking and Antigen Presentation in the Human Immune Response to
749 Mycobacterium tuberculosis . *The Journal of Immunology*, *173*(1), 494–506.
750 https://doi.org/10.4049/jimmunol.173.1.494

751 Mayer-Barber, K. D., Andrade, B. B., Barber, D. L., Hieny, S., Feng, C. G., Caspar, P., …
752 Sher, A. (2011). Innate and adaptive interferons suppress IL-1α and IL-1β production by
753 distinct pulmonary myeloid subsets during Mycobacterium tuberculosis infection.
754 *Immunity*, *36*(6), 1023–1034. https://doi.org/10.1038/jid.2014.371

Mayer-Barber, K. D., Andrade, B. B., Oland, S. D., Amaral, E. P., Barber, D. L., Gonzales, J., … Sher, A. (2014). Host-directed therapy of tuberculosis based on interleukin-1 and type I interferon crosstalk. *Nature*, *118*(24), 6072–6078. https://doi.org/10.1002/cncr.27633.Percutaneous

Mayer-Barber, K. D., & Barber, D. L. (2015). Innate and adaptive cellular immune responses to Mycobacterium tuberculosis infection. In *Cold Spring Harbor Perspectives in Medicine* (Vol. 5). https://doi.org/10.1101/cshperspect.a018424

Mayer-Barber, K. D., Barber, D. L., Shenderov, K., White, S. D., Wilson, M. S., Cheever, A., … Sher, A. (2010). Cutting Edge: Caspase-1 Independent IL-1β Production Is Critical for Host Resistance to Mycobacterium tuberculosis and Does Not Require TLR Signaling In Vivo . *The Journal of Immunology*, *184*(7), 3326–3330. https://doi.org/10.4049/jimmunol.0904189

Mcdonough, K. A., Kress, Y., & Bloom, B. R. (1993). Pathogenesis of Tuberculosis : Interaction of Mycobacterium tuberculosis with Macrophages. *Infection and Immunity*, *61*(7), 2763–2773.

Muruganandah, V., Sathkumara, H. D., Navarro, S., & Kupz, A. (2018). A Systematic Review: The Role of Resident Memory T Cells in Infectious Diseases and Their Relevance for Vaccine Development. *Frontiers in Immunology*, *9*(July). https://doi.org/10.3389/fimmu.2018.01574

Mwandumba, H. C., Russell, D. G., Nyirenda, M. H., Anderson, J., White, S. A., Molyneux, M. E., & Squire, S. B. (2004). Mycobacterium tuberculosis Resides in Nonacidified Vacuoles in Endocytically Competent Alveolar Macrophages from Patients with Tuberculosis and HIV Infection 1. *The Journal of Immunology*.

Myrvik, Q. N., Leake, E. S., & Wright, M. J. (1984). Disruption of phagosomal membranes by the H37Rv strain of Mycobacterium tuberculosis. A correlate of virulence. *Am Rev Respir Dis*, *129*(2), 322–328.

781 Pym, A. S., Brodin, P., Majlessi, L., Brosch, R., Demangel, C., Williams, A., … Cole, S. .
782 (2003). Recombinant BCG exporting ESAT-6 confers enhanced protection against
783 tuberculosis. *Nature Medicine*, *9*(5), 533–539. https://doi.org/10.1038/nm

784 Queval, C. J., Brosch, R., & Simeone, R. (2017). The Macrophage : A Disputed Fortress in
785 the Battle against Mycobacterium tuberculosis. *Frontiers in Microbiology*, pp. 1–11.
786 https://doi.org/10.3389/fmicb.2017.02284

787 Quigley, J., Hughitt, V. K., Velikovsky, C. A., Mariuzza, R. A., El-Sayed, N. M., & Briken, V.
788 (2017). The cell wall lipid PDIM contributes to phagosomal escape and host cell exit of
789 Mycobacterium tuberculosis. *MBio*, *8*(2), 1–12. https://doi.org/10.1128/mBio.00148-17

790 Rothchild, A. C., Olson, G. S., Nemeth, J., Amon, L. M., Mai, D., Gold, E. S., … Aderem, A.
791 (2019). Alveolar macrophages generate a non-canonical NRF2-driven transcriptional
792 response to Mycobacterium tuberculosis in vivo. *Science Immunology*, *4*(37).
793 https://doi.org/10.1016/j.physbeh.2017.03.040

794 Russell, D. G., Mwandumba, H. C., & Rhoades, E. E. (2002). Mycobacterium and the coat of
795 many lipids. *Journal of Cell Biology*, *158*(3), 421–426.
796 https://doi.org/10.1083/jcb.200205034

797 Russell, D. G., Vanderven, B., Glennie, S., Mwandumba, H., & Heyderman, R. (2009). The
798 macrophage marches on its phagosome: dynamic assays of phagosome function. *Nat*
799 *Rev Immunol*, *9*(8), 594–600. https://doi.org/10.1038/nri2591.The

800 Samstein, M., Schreiber, H. A., Leiner, I. M., Sušac, B., Glickman, M. S., & Pamer, E. G.
801 (2013). Essential yet limited role for CCR2+ inflammatory monocytes during
802 Mycobacterium tuberculosis-specific T cell priming. *ELife*.
803 https://doi.org/10.7554/eLife.01086

804 Sayes, F., Blanc, C., Ates, L. S., Deboosere, N., Orgeur, M., Le Chevalier, F., … Majlessi, L.
805 (2018). Multiplexed Quantitation of Intraphagocyte Mycobacterium tuberculosis

Secreted Protein Effectors. *Cell Reports*, *23*(4), 1072–1084. https://doi.org/10.1016/j.celrep.2018.03.125

Sharma, R., Lahiri, R., Scollard, D. M., Pena, M., Williams, D. L., Adams, L. B., … Truman, R. W. (2013). The armadillo: A model for the neuropathy of leprosy and potentially other neurodegenerative diseases. *DMM Disease Models and Mechanisms*, *6*(1), 19–24. https://doi.org/10.1242/dmm.010215

Simeone, R., Bobard, A., Lippmann, J., Bitter, W., Majlessi, L., Brosch, R., & Enninga, J. (2012). Phagosomal rupture by Mycobacterium tuberculosis results in toxicity and host cell death. *PLoS Pathogens*, *8*(2). https://doi.org/10.1371/journal.ppat.1002507

Simeone, R., Sayes, F., Song, O., Gröschel, M. I., & Brodin, P. (2015). Cytosolic Access of Mycobacterium tuberculosis : Critical Impact of Phagosomal Acidification Control and Demonstration of Occurrence In Vivo. *PLOS Pathogens*, 1–24. https://doi.org/10.1371/journal.ppat.1004650

Srinivasan, L., Gurses, S. A., Hurley, B. E., Miller, J. L., Karakousis, P. C., & Briken, V. (2016). Identification of a Transcription Factor That Regulates Host Cell Exit and Virulence of Mycobacterium tuberculosis. *PLoS Pathogens*, *12*(5), 1–29. https://doi.org/10.1371/journal.ppat.1005652

Stamm, L. M., Morisaki, J. H., Gao, L. Y., Jeng, R. L., McDonald, K. L., Roth, R., … Brown, E. J. (2003). Mycobacterium marinum Escapes from Phagosomes and Is Propelled by Actin-based Motility. *Journal of Experimental Medicine*, *198*(9), 1361–1368. https://doi.org/10.1084/jem.20031072

Sturgill-Koszycki, S., Schlesinger, P. H., Chakraborty, P., Haddix, P. ., Collins, H. ., Fok, A. ., … Russell, D. G. (1994). Lack of acidification in Mycobacterium phagosomes produced by exclusion of the vesicular proton-ATPase. *Science*, *263*(5147), 678–681.

Sundaramurthy, V., Korf, H., Singla, A., Scherr, N., Nguyen, L., Ferrari, G., … Pieters, J.

(2017). Survival of Mycobacterium tuberculosis and Mycobacterium bovis BCG in lysosomes in vivo. *Microbes and Infection*, *19*(11), 515–526. https://doi.org/10.1016/j.micinf.2017.06.008

van der Wel, N. N., Fluitsma, D. M., Dascher, C. C., Brenner, M. B., & Peters, P. J. (2005). Subcellular localization of mycobacteria in tissues and detection of lipid antigens in organelles using cryo-techniques for light and electron microscopy. *Current Opinion in Microbiology*, *8*(3), 323–330. https://doi.org/10.1016/j.mib.2005.04.014

van der Wel, N. N., Hava, D., Houben, D., Fluitsma, D., van Zon, M., Pierson, J., … Peters, P. J. (2007). M . tuberculosis and M . leprae Translocate from the Phagolysosome to the Cytosol in Myeloid Cells. *Cell*, 1287–1298. https://doi.org/10.1016/j.cell.2007.05.059

van Leeuwen, L. M., Boot, M., Kuijl, C., Picavet, D. I., van Stempvoort, G., van der Pol, S. M. A., … Bitter, W. (2018). Mycobacteria employ two different mechanisms to cross the blood–brain barrier. *Cellular Microbiology*, *20*(9), 1–17. https://doi.org/10.1111/cmi.12858

Vandal, O. H., Nathan, C. F., & Ehrt, S. (2009). Acid resistance in Mycobacterium tuberculosis. *Journal of Bacteriology*, *191*(15), 4714–4721. https://doi.org/10.1128/JB.00305-09

Vaziri, F., & Brosch, R. (2019). ESX / Type VII Secretion Systems — An Important Way Out for Mycobacterial Proteins. *Microbiol Spectrum*, *7(4):PSIB*-(PSIB-0029-2019). https://doi.org/10.1128/microbiolspec.PSIB-0029-2019.Correspondence

Vieira, O. V., Botelho, R. J., & Grinstein, S. (2002). Phagosome maturation: aging gracefully. *Biochemical Journal*, *366*(3), 689–704. https://doi.org/10.1042/bj20020691

Wassermann, R., Gulen, M. F., Sala, C., Perin, S. G., Lou, Y., Rybniker, J., … Ablasser, A. (2015). Mycobacterium tuberculosis Differentially Activates cGAS- and Inflammasome-Dependent Intracellular Immune Responses through ESX-1. *Cell Host and Microbe*,

17(6), 799–810. https://doi.org/10.1016/j.chom.2015.05.003

Watson, R. O., Bell, S. L., MacDuff, D. A., Kimmey, J. M., Diner, E. J., Olivas, J., … Cox, J. S. (2015). The cytosolic sensor cGAS detects Mycobacterium tuberculosis DNA to induce type I interferons and activate autophagy. *Cell Host Microbe*, *17*(6), 811–819. https://doi.org/110.1016/j.bbi.2017.04.008

Weerdenburg, E. M., Abdallah, A. M., Mitra, S., De Punder, K., Van der Wel, N. N., Bird, S., … Van der Sar, A. M. (2012). ESX-5-deficient Mycobacterium marinum is hypervirulent in adult zebrafish. *Cellular Microbiology*, *14*(5), 728–739. https://doi.org/10.1111/j.1462-5822.2012.01755.x

Wong, D., Bach, H., Sun, J., Hmama, Z., & Av-gay, Y. (2011). Mycobacterium tuberculosis protein tyrosine to inhibit phagosome acidification. *PNAS*, *108*(48), 19371–19376. https://doi.org/10.1073/pnas.1109201108

World Health Organization. (2019). *Global Tuberculosis Report 2019: Fact sheet*. https://doi.org/10.1017/CBO9781107415324.004

Yamada, H., Mizuno, S., Horai, R., Iwakura, Y., & Sugawara, I. (2000). Protective role of interleukin-1 in mycobacterial infection in IL-1 alpha/beta double knockout mice. *Lab Invest*, *80*, 759–767.

Young, D. C., Layre, E., Pan, S., Tapley, A., Adamson, J., Wu, Z., … Moody, D. B. (2015). chemical markers of Mycobacterium tuberculosis infection. *Chem Biol.*, *22*(4), 516–526. https://doi.org/10.1016/j.chembiol.2015.03.015.In